



Tropical tree size–frequency distributions from airborne lidar

ANTÓNIO FERRAZ ^{1,2,5} SASSAN S. SAATCHI,^{1,2} MARCOS LONGO ³ AND DAVID B. CLARK⁴

¹Jet Propulsion Laboratory, California Institute of Technology, Pasadena, California 91109 USA

²Institute of Environment and Sustainability, University of California, Los Angeles, California 90024 USA

³NASA Postdoctoral fellow, Jet Propulsion Laboratory, California Institute of Technology, Pasadena, California 91109 USA

⁴Department of Biology, University of Missouri-St. Louis, St. Louis, Missouri 63121 USA

Citation: Ferraz, A., S. S. Saatchi, M. Longo, and D. B. Clark. 2020. Tropical tree size–frequency distributions from airborne lidar. *Ecological Applications* 00(00):e02154. 10.1002/eap.2154

Abstract. In tropical rainforests, tree size and number density are influenced by disturbance history, soil, topography, climate, and biological factors that are difficult to predict without detailed and widespread forest inventory data. Here, we quantify tree size–frequency distributions over an old-growth wet tropical forest at the La Selva Biological Station in Costa Rica by using an individual tree crown (ITC) algorithm on airborne lidar measurements. The ITC provided tree height, crown area, the number of trees >10 m height and, predicted tree diameter, and aboveground biomass from field allometry. The number density showed strong agreement with field observations at the plot- (97.4%; 3% bias) and tree-height-classes level (97.4%; 3% bias). The lidar trees size spectra of tree diameter and height closely follow the distributions measured on the ground but showed less agreement with crown area observations. The model to convert lidar-derived tree height and crown area to tree diameter produced unbiased (0.8%) estimates of plot-level basal area and with low uncertainty (6%). Predictions on basal area for tree height classes were also unbiased (1.3%) but with larger uncertainties (22%). The biomass estimates had no significant bias at the plot- and tree-height-classes level (–5.2% and 2.1%). Our ITC method provides a powerful tool for tree- to landscape-level tropical forest inventory and biomass estimation by overcoming the limitations of lidar area-based approaches that require local calibration using a large number of inventory plots.

Key words: airborne lidar; crown area; individual tree crown; plot-level aboveground biomass; size-classes-level basal area; tree diameter; tree height; tree size frequency.

BACKGROUND

A combination of biological and ecological processes governs humid tropical forest structure and demography that in turn control the water, carbon, and energy fluxes at the ecosystem level. The distribution of tree size, canopy cover and gaps, and the complex diversity of structure strongly influence the response and resilience of tropical ecosystems to climate stress (Levine et al. 2016, Longo et al. 2018, McDowell et al. 2018) and land use pressures (Bustamante et al. 2016, Nobre et al. 2016). In particular, improved representations of forest structure and size distribution across the landscape in dynamic ecosystem models are considered critical for a more realistic prediction of current state and future evolution of the ecosystem function (Fisher et al. 2018).

In the absence of direct observation of forest structure at the landscape level, several theories have been developed to describe and predict the variations of forest structure and size distributions in different ecosystems. For example, metabolic scaling theory based on

hydraulic constraints propose that size–density distribution of natural and undisturbed forest in equilibrium should follow a power-law scaling with respect to tree diameter across all forest types (Enquist and Niklas 2001, Enquist et al. 2009). This theory also predicts a constant logarithmic scaling between tree height and trunk diameter, with an exponent close to 2/3 (Enquist and Niklas 2001, West et al. 2009). However, in most natural tropical ecosystems that deviate from a steady-state condition due to past disturbance and climate induced responses, and particularly for large trees, the theory may not be able to predict the observations (Muller-Landau et al. 2006a, Farrior et al. 2016). Furthermore, empirical studies suggest that there are significant intraspecific (Poorter et al. 2003, Bohlman and O'Brien 2006) and intersite variability (Coomes et al. 2003, Muller-Landau et al. 2006b, Lau et al. 2019) in tree crown architectural development in tropical forests that cannot be readily predicted by scaling theory. In particular, the tree diameter–height relationship is subject to strong intersite variability, which might be related to environmental conditions, floristic composition, nutrient availability, and soil type (Nogueira et al. 2006, Feldpausch et al. 2011, Banin et al. 2012, Molto et al. 2014). There is also strong evidence in forest inventory data for intrasite

Manuscript received 19 August 2019; revised 26 March 2020; accepted 30 March 2020. Corresponding Editor: Nancy F. Glenn.

⁵E-mail: Antonio.A.Ferraz@jpl.nasa.gov

variability on the diameter–crown-size relationship across space and functional groups (e.g., shade-tolerant, partial-shade-tolerant, long-lived pioneer, Bohlman and O’Brien 2006, Blanchard et al. 2016, Cano et al. 2019). Natural and anthropological disturbance processes further limit the transferability of the scaling theory across the landscape.

Variations in tree morphology reflect the magnitude of the actual responses of trees to the availability of soil nutrient resources, climate conditions, and local spatial crowding (Iwasa et al. 1985, Poorter et al. 2003, Kitajima et al. 2005). We still do not know at what scales these variations occur, i.e., whether micro or macro features are driving forest structure and demographics, and if the variations can be predicted accurately with environmental and nutrient variables. Field inventory systems seldom characterize tree size distribution variability at the landscape level due to the limited number of plots that are either small or sparse across the landscape. In field-based techniques, the three-dimensional forest structure is usually approximated by considering the tree diameter as a proxy for both horizontal and vertical expansion of trees. If the diameter increases continuously with the age of tree due to xylem expansion, we still do not understand which changes may covary with the diameter increment in terms of resource allocation to tree height growth and crown expansion (Blanchard et al. 2016). The collection of field sampled tree height and crown size have been increasing in the last years to fulfill the needs of different applications such as developing the allometric models for predicting volume structure and above-ground biomass or improve the parametrization of vegetation dynamic models (Chave et al. 2014, Fisher et al. 2018). However, there are large uncertainties associated with forest structure such as the crown morphology, gap dynamics, and individual tree height and growth rates that are difficult to measure in the field in extensive spatial and temporal scales. Therefore, the observations to quantify the forest demography and disturbance, basal area, tree height and crown-size–frequency distributions across landscapes remain a challenging problem for field ecologists.

In this study, we use high spatial resolution airborne laser scanning to model individual trees crowns (ITC) and to retrieve tree size–frequency distributions at the landscape scale. Lidar-based methods have been used to sample individual trees over different forest biomes but there was no method to deal with the complexity of tropical forests structures. We recently developed an algorithm that was successful to extract and model trees for every forest layer using the adaptive mean shift technique (AMS3D, Ferraz et al. 2016). Our method clusters lidar point clouds (photons returning from different tree components) into 3D models of individual trees with direct information about tree height, crown size, and the number of trees, and indirect inference of additional structural traits such as stem diameter, carbon and leaf

area index (LAI) using local or general allometry. The detailed size–frequency distributions (or size spectrums) provides structural traits and their scaling mechanisms (tree to forest to landscape scales) to study different ecological processes such as biomechanics, energy and material flux, tree competition, crown expansion (West et al. 2009). The technique, once applied to repeated lidar observations, can inform a suite of ecological applications (e.g., tree demography, forest disturbance and recovery, carbon fluxes).

To demonstrate the ITC and AMS3D techniques, we use lidar observations over a tropical rain forest in the La Selva Biological Station, Costa Rica to extract tree size–frequency distributions and compare the results with ground measurements. The spatial information produced from lidar data are validated with field estimates on tree density, basal area, aboveground biomass, and size spectra of tree height, stem diameter, and crown area. We investigate potential landscape-scale bias by assessing results at the plot- and tree-height-classes level. We directly compare field and lidar observations on tree height to assess whether errors are associated with forest structure (e.g., forest height, canopy cover) and/or topographic features (e.g., slope, elevation). We study the impact of allometric equations (e.g., local vs. regional) in estimating stem diameter and basal area from lidar-derived tree structural traits (height and crown area). The last goal is to test the capabilities of the AMS3D to capture the tree density and tree traits variability across forests with different historical disturbances and soil conditions (old-growth forest, selectively logged forest, secondary forest, and forest in swamp areas).

MATERIALS AND METHODS

Study site

The La Selva Biological Station is a 1,536-ha research station located in the Atlantic lowlands of northeastern Costa Rica (Fig. 1). The elevation ranges between 39.6 m and 150.8 m (average equals 79 m) above sea level with a dominant southwest-northeast gradient resulting in higher elevations in the border with Braulio Carrillo National Park (Appendix S1: Fig. S1a). The slope variations (0–76° with an average of 13°) within the study area are dominated by microtopography with a general trend that increases in the northeast-southwest direction (Appendix S1: Fig. S1b). La Selva receives average annual rainfall of 4,000 mm and mean temperature of 26°C. The study area is covered by a mixture of old growth and secondary lowland wet tropical forests along with swamp forest, remnant plantations, and various agroforestry treatments (Fig. 1). The soil is dominated by a mixture of inceptisols (namely in alluvial terraces) in the north and residual ultisols to the south (Drake et al. 2002, Clark et al. 2010). Over its 62-yr history, La Selva has become one of the most extensively studied field sites in tropical forests with well-

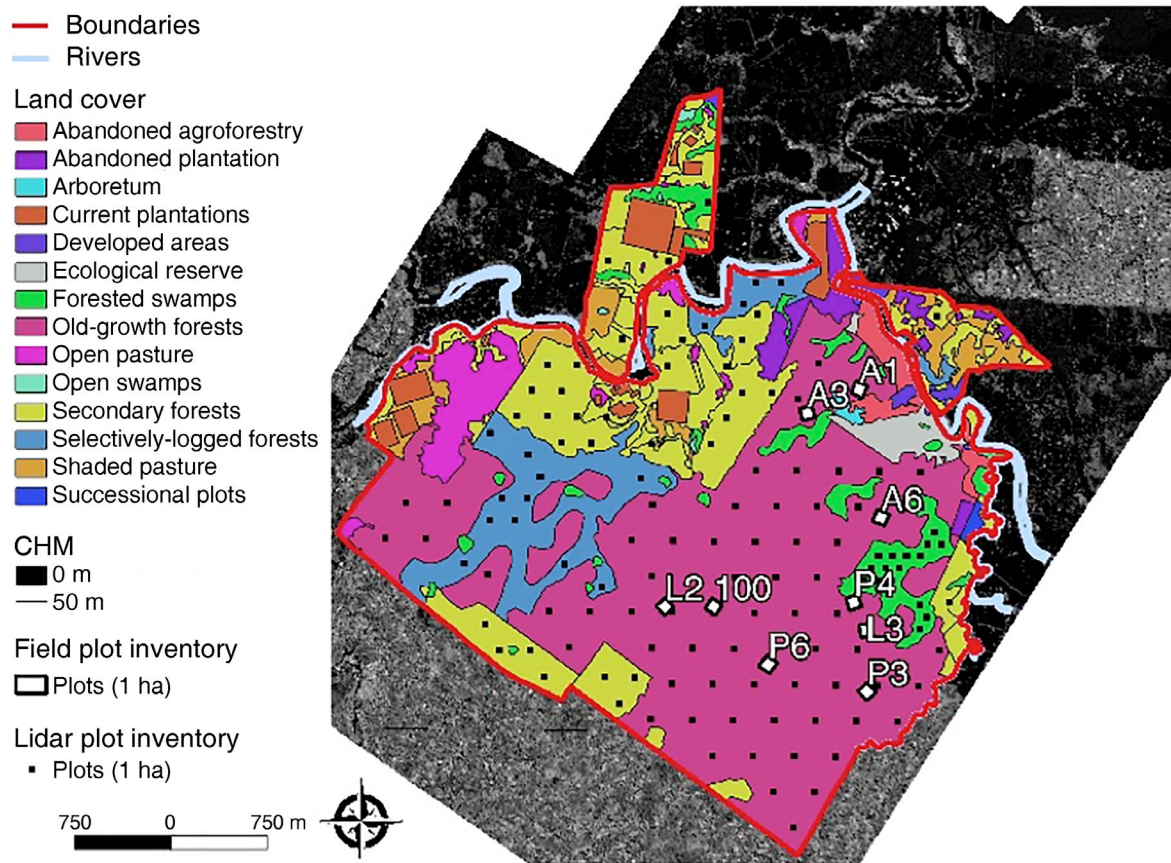


FIG. 1. La Selva biological station boundaries and land cover map overlapped to a canopy height model (see Appendix S1: Fig. S1d for detailed view). Field plots (1 ha) are shown in white squares. The black squares correspond to a systematic sampling of 1-ha plots over the lidar coverage that is used to study the lidar-derived tree size and density variability across different land forest types, namely old-growth, secondary, selectivity-logged and swamp forests (see *Variation of tree-size-frequency distributions across forest types*). The black squares are not shown in real size for visualization purposes.

documented ecological and biological data sets (Bawa et al. 1994).

Field inventory

The field sampling was based in a long-term inventory called the CARBONO project (Clark et al. 2017) that originally included 18 0.5 ha (50×100 m) permanent plots located in old-growth forest using a stratified random design in three edaphic conditions: flat site on old alluvial soils, flat sites on residual soils, and steeply sloping plots on residual soils (Clark et al. 2010, Appendix S1: Fig. S1c). Individual trees were characterized using several traits that included tree location, species, tree diameter (D), and whether they were alive or dead. In 2009, 12 out of the 18 plots were extended to cover 1 ha in order to better integrate with remote sensing applications. Tree height (H) was measured in addition to the traditional metrics over 8 of these 12 plots (denoted by letters in Fig. 1) by using a laser rangefinder mounted in a tripod from the furthest distance with

good visibility to the tree apex (see Appendix S1: Section S2.2). In 2013, an additional plot (plot “100”, Fig. 1) was measured following the same protocol with supplementary observations of crown radius (CR) for a subsample of trees within the plot. CR was estimated visually from eight compass-measured cardinal and intercardinal directions using a clinometer to determine the ground position vertically below each point; slope-corrected distance to the trunk was measured and the trunk radius added to calculate each radius. Using a size-stratified random sampling approach, we developed unbiased measurement of CR across tree size classes within the plot (see Appendix S1: Section S2.3). The randomization was based on the trunk diameter, assuming crown size and condition vary with the trunk size. We calculated crown area (CA) using the area of the convex hull that encloses all the points. In 2016, the same protocol was used to sample crown size for plots A1, A4, L1, and P1. In this work, we use nine plots that included H measurements for comparison with the remote sensing approach (Fig. 1). In summary, we used

4,311 trees ($H \geq 10$ m) that have been characterized by their GPS location, D and H , and 285 trees among them with additional estimates of CA .

Airborne lidar observation and tree crown extraction

The Blom Corporation and Northrop Grumman Company collected the lidar data in 2009 using an Optech ALTM 3100 (Teledyne Optech, Toronto, Canada) scanning device with a laser beam density of 6 points/m². The lidar data were processed to provide geo-referenced point clouds and further to classify ground and off-ground points (Soininen 2011). We used a Delaunay triangulation calculated from the ground points to model the surface in order to estimate the distance to the ground for every lidar point and remove the effect of topography by assigning the corresponding height to each point. The adaptive mean shift algorithm (AMS3D, Ferraz et al. 2016) is applied to decompose the lidar point cloud into clusters that correspond to individual tree crowns (ITC) providing a full characterization of the different layers of vegetation such as emergent or dominated (Fig. 2). The estimated processing time for each 1-ha plot averaging 6 points/m² is of 4.9 h (see Appendix S1: Section S9). The position of a tree is given by the planimetric barycenter of the corresponding lidar points, while the H is referred to the highest lidar point. To calculate CA , we first project the crown points in the x – y plane and then we calculate the corresponding alpha shape ($\alpha = 2$). The CR is calculated by averaging the distances between the centroid and boundaries of the alpha shapes according to height pre-determined directions that match the eight principal directions of a compass rose. Additional metrics (e.g., crown volume, crown base height) are also directly estimated from the ITC calculated by the AMS3D method but are not used in this study.

Tree size allometry

We develop several local allometric models to convert direct lidar-derived tree H and CA into D . Similarly, we developed models to convert field measurements of D and H into estimates of CA . Allometric equations are generally developed by fitting ordinary least squares linear regressions to field inventory data that are usually log-transformed to address the heteroscedasticity of residuals. This approach might still present large bias in the characterization of large trees because the field sampling distribution is highly skewed as small stems vastly outnumber large ones. Here, we test allometric regression models derived from either binned or raw data to address the skewedness of the sampling (see Appendix S1: Section S5). We follow the methodology presented in Jucker et al. (2017) to propagate the uncertainty in the binned model predictions. The tree structural traits were regressed against each other either individually or combined in order to select the best predictors. In addition, we tested models that follow power-

law, exponential, logarithm, and linear growth functions. The models that best explain each tree size relationships are selected using the lowest root mean square error (RMSE, see Appendix S1: Section S5).

Tree size–frequency distributions

The validation of lidar ITC using field inventory by matching lidar and ground trees is prone to errors as the approaches estimate tree metrics with different magnitudes of uncertainties (see Appendix S1: Section S3). Tree D is relatively easy to measure in the field except for irregular trees with buttresses or with vines and lianas. Lidar measurements estimate D using allometric models but with large uncertainties associated particularly for large trees. In contrast, lidar provide more accurate estimates of tree location (often measured using handled GPS devices in field techniques) and H . La Selva is an optimal location to validate our products because the field inventory offers measurements of H for every tree ($D > 10$ cm) in nine 1-ha plots. Uncertainties in the field measurements are due to human errors, obscured visibility of tree crown tops for H and CA , and the tree diameter above the buttress (50 cm above the buttress at the cylindrical part of the stem), which is an a priori determined standard approach to estimate the equivalent diameter used in the biomass allometry (Chave et al. 2005, 2014).

Using common tree metrics measured from both field and lidar techniques allows us to calibrate any potential bias between measurements. For instance, in this work, we set a height threshold ($H > 10$ m) to compare tree density results. The conversion of field estimated D into H from allometric models to define a height threshold could directly impact the comparison of tree number density because a small uncertainty of just a few centimeters in D can readily translate into a significant number (e.g., >10% individuals) in small trees (see Appendix S1: Section S4). A one-to-one comparison of individual trees from lidar and ground would require a search methodology to match between individual trees of the two data sets. Except for the emergent trees, such methodology would be difficult to implement due to the uncertainty associated to each technique in estimating specific tree structural variables (see Appendix S1: Section S3). Therefore, for comparison between the plot and lidar estimates of individual H , we developed ranked-based Q-Q plots by sorting H in decreasingly order for each plot, matching the tallest lidar tree with the tallest tree in the field inventory, and going down the list until, there is no additional trees in either field- or lidar-based data sets (see Appendix S1: Section S4 and Fig. S2). Although this is not a direct approach for matching the trees, the methodology allows us to estimate a plot-level correction factor to minimize the bias between the data sets. From the matching, we calculate a regression model for the plot-level relationship between field- and ITC-derived H and apply the fitted model to

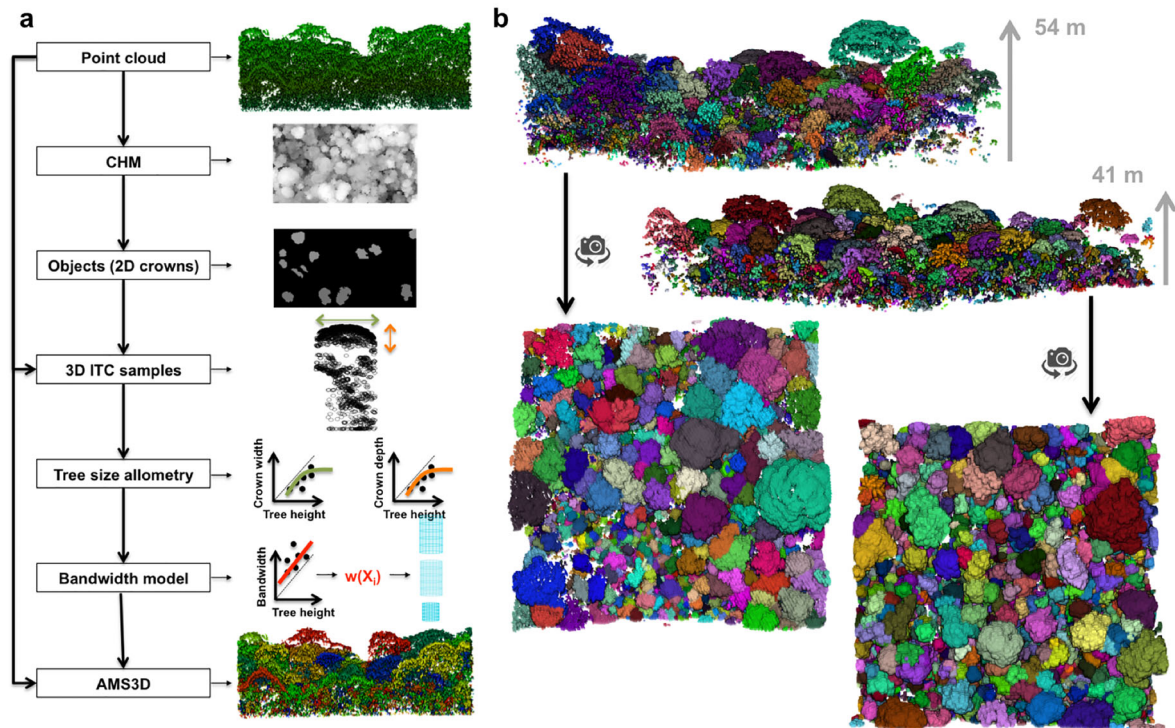


FIG. 2. Adaptive mean shift (AMS3D; Ferraz et al 2016) (a) workflow and (b) examples of individual tree crown (ITC) extraction over 150×50 m plots.

the lidar data set to obtain unbiased height estimates relative to the field measurements (Larjavaara and Muller-Landau 2013).

Tree size–frequency information inferred from the lidar are verified using similar data from field inventory measurements in nine 1-ha plots. We compare tree density and tree-size spectra (or size–abundance distribution; White et al. 2007) for three structural traits of H , D , and CA . The size spectra are calculated through a commonly used approach that sorts the ITC traits in a decreasing order and assigns an index to each tree in the population. The tree with the largest size of a given structural trait receives index = 1, and the smallest size tree an index equal to the number of trees in the plot. By plotting the trait size (x -axis) against the index (y -axis) we draw a size–abundance profile from which we can read how many individuals exist for a given trait size range. The size spectra comparison and analysis demonstrate the performance of the lidar AMS3D data to estimate tree size frequencies across the landscapes, particularly in separating the large and small trees in the forest. In addition to the plot-level size spectra analysis, we calculate the landscape-scale size–frequency distribution to assess any potential bias in the AMS3D estimates when aggregating results across the study region. We investigate the errors and bias associated with estimating basal area from the ITC by aggregating trees at the plot-level as well as according to

size classes of 5 m height intervals. It assesses the AMS3D reliability to estimate landscape-scale basal area in the spatial and size spectrum domains. We do a similar analysis for aboveground biomass by using tree-level estimates that are derived from D together with a reference allometry that has been widely applied to field measurements in the La Selva Biological Station (Brown 1977; see Appendix S1: Section S7). Finally, we compare tree size distributions and variability of forest structure across different forest types across La Selva Biological Station, including old-growth, secondary, selectively logged, and swamp forests.

RESULTS AND DISCUSSION

Tree size allometry

The field allometric models developed to estimate tree diameter (D) and crown area (CA) are shown in Table 1 and Fig. 3 (refer to Appendix S1: Section S5 for additional local allometries). Power-law models defined as a function of two structural traits were preferred to allometry based on a single trait and/or following different growth functions (Appendix S1: Tables S1 and S2). The most explanatory models have significant uncertainties of $RMSE = 8.8$ cm ($\sim 23\%$) and $RMSE = 24.67$ m² ($\sim 38\%$) for D and CA , respectively.

TABLE 1. Tree size allometry based on the field inventory.

Model	α	β	RMSE (m)	Bias (m)	CV (%)	Eq.
$D = \alpha (H \times CA)^\beta$	1.62	0.43	8.8	−2.1	23.23	1
$CA = \alpha (D \times H)^\beta$	0.42	0.73	24.67	−1.52	37.55	2

Notes: α includes the correction factor to account for the back-transformation of the regression error (Baskerville 1972). CV (%) has been calculated using a bootstrapped cross-validation ($n = 100$) with replacement using 30% (10% for CA, see Appendix S1: Section S5) of the observations for validation. CA, crown area; D , tree diameter; H , tree height. Refer to Appendix S1: Section S5 for additional allometric models and details on the model calculation and selection.

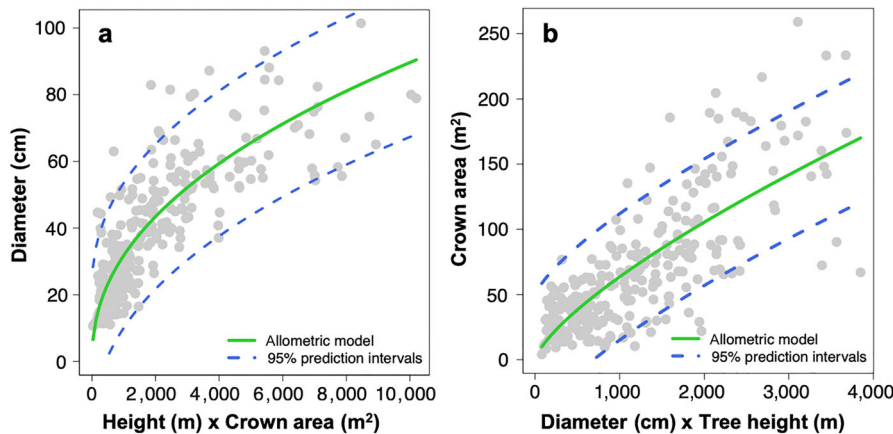


FIG. 3. Local tree size allometry derived from field observation to estimate (a) tree diameter (Table 1: Eq. 1) and (b) crown area (Table 1: Eq. 2). Please refer to Appendix S1: Section S5 for details on the model’s development and additional local allometry (Appendix S1: Tables S1 and S2).

The overall accuracy of the models shows two distinct features. For trees with $D < 50$ cm, the uncertainty remains limited (16% and 32% for D and CA, respectively) whereas it is substantially larger (31% and 69%) for trees $D > 50$ cm. This suggests that during the early successional stages the tree structural traits follow a more predictable trajectory. As trees become larger, they develop irregular shapes, and both the D and CA disperse from any trajectory and follow a more unpredictable growth rate that depend strongly on the gap dynamics, light condition, packing density, soil nutrients, topographical variations, and disturbance effects such as branch mortality by natural causes or external factors (e.g., wind, lightning; Negrón-Juárez et al. 2018, Yanoviak et al. 2019). These factors influence the height–diameter relationship and CA asymptotes to a saturation point for most tree species (Muller-Landau et al. 2006a, West et al. 2009).

Lidar tree height calibration

A plot-level H correction factor close to one indicates a better match between the two data sets (see *Tree size–frequency distributions* and Appendix S1: Section S4). In practice, the index ranges between 0.77 and 1 and has a strong correlation with surface elevation, suggesting any mismatch between the two data sets is worse at lower

elevations (Fig. 4a). The H correction factor is also strongly correlated with the height of the tallest trees within the plots (Fig. 4b). In general, the field measurements overestimated the tree height compared with the lidar with increasing differences for taller trees ($H > 30$ m, Appendix S1: Fig. S2). Plot 100 has a systematic error along the entire height spectrum due to the fact that trees were measured 4 yr after the lidar measurements.

We suspect that there might be a larger uncertainty in measuring H of tall trees using laser rangefinders because the tree apex is harder to identify from the ground at short distances and, it requires larger observing angles that are more sensitive than small angles in terms of propagation of the errors to estimate tree height (Larjavaara and Muller-Landau 2013). Hunter et al. (2013) reported that handheld clinometer observations overestimated by 1.4 m the lidar measurements of H in three Brazilian Amazon’s sites. Repeated field estimates on 174 trees (averaged errors of 1.1 m, standard deviation of 4.7 m) lead to the conclusion that larger uncertainties are associated with taller trees. Wang et al. (2019) found that field measurements systematically overestimate H of a boreal forest compared with airborne lidar. Larjavaara and Muller-Landau (2013) estimated H of trees in Barro Colorado Island (BCI), Panama, by climbing neighborhood towers and stopping

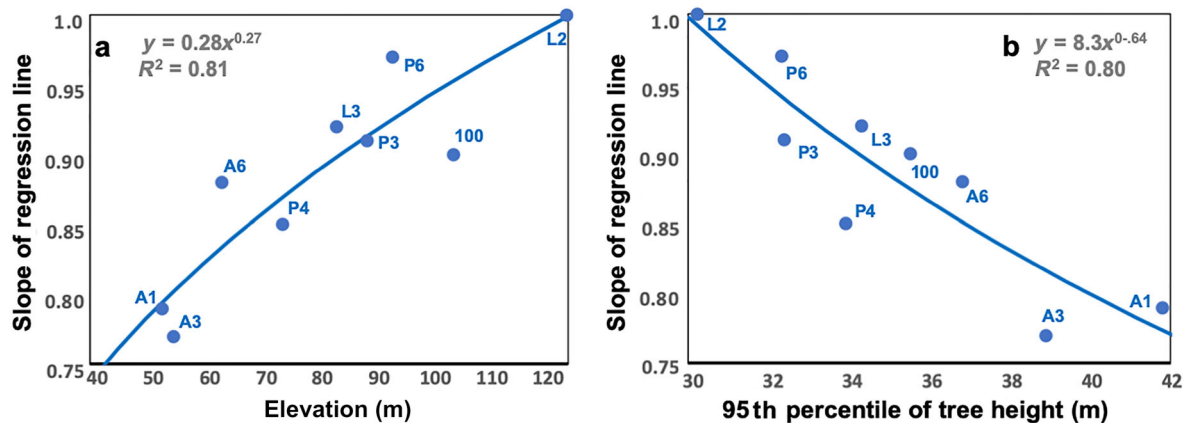


FIG. 4. Relationship between (a) the plots elevation and (b) the 95th percentile of individual tree height (H) and the H correction factor used to compensate for the bias between field and lidar estimates. The H correction factor is derived from the slope of linear regression models calculated from ranked-based Q-Q plots (Appendix S1: Section S4 and Fig. S2).

when reaching the tree apex height level to find the opposite trend of the aforementioned works, i.e., the laser rangefinder underestimates the reference H .

Comparison of lidar and forest inventory data

The AMS3D provides spatially explicit distributions of tree H and D that strongly follow the patterns mapped by the field inventory (Appendix S1: Figs. S7 and S8). Fig. 5 shows examples of H distribution maps over plots with a variety of forest structure and tree size spectra that have been successfully modeled by the AMS3D. For instance, plots A1 and A6 are dominated by tall trees and have lower tree density (293 and 333 trees/ha, respectively, Fig. 6) compared with plots L2 and P6 (527 and 480 trees/ha, respectively) that are characterized by higher densities and shorter trees. Mapping tree size distribution at the landscape scale across heterogeneous forest structures is crucial to investigate scale-related questions in forest ecology, especially the response of plants to habitat change occurring at a variety of spatial and temporal scales (Crowther et al 2015, Schimel et al. 2019).

Tree density.—There is a strong correlation ($R^2 = 0.88$) between AMS3D and field estimates in terms of plot-scale tree density ($H > 10$ m, Fig. 6a). Results are nearly unbiased (bias = 2.8%) with an RMSE = 6.4%. The averaged detection rate is highly satisfactory ($97.4\% \pm 5.6\%$) with plot-level errors bounded by 10%. It shows the consistency of the AMS3D to estimate tree density across plots of old-growth forest with a significant demographic variability that ranges from 293 trees/ha (plot A1) to 527 trees/ha (plot L2). The averaged detection rate across the height classes is also high ($94.7\% \pm 17.2\%$) but has a large variability along the tree height range (Fig. 6b). This might be related with the discrepancy between field and lidar techniques in

measuring tree height that allocates trees to different height classes. Nevertheless, results indicate that the plot-level H calibration (see *Lidar tree height calibration*) is relatively successful for the entire tree height size spectrum (Fig. 6b). Compared with the plot-level approach, the RMSE (11.5%) is larger but results remain nearly unbiased (2.8%). The unbiased results ensure that the AMS3D is a reliable tool to map tree density variability at the landscape scale across forest plots and tree size classes. The availability of tree size frequency distributions along space and time enables the study of a myriad of applications such as tree recruitment, tree competition, and forest disturbance.

The validation of lidar results in terms of tree density is highly sensitive to the height threshold used to select the trees that are visible on the lidar data set due to the fact that small trees largely outnumber the large trees. For instance, the height of nearly 20% of the trees in our study site are within the interval of $10 \text{ m} < H < 13 \text{ m}$ and therefore a small bias between field and lidar estimates can lead to errors up to 20%. With the H correction factor (see *Lidar tree height calibration*), the tree density accuracy increased significantly from the bias (9.9%) and errors (RMSE = 14.8%, refer to Appendix S1: Figs. S4 and S5). The availability of a common metric between the field and lidar measurements is crucial to assess the results of lidar ITC methods as it allows us to calibrate the observations without introducing additional uncertainty from the allometric equations used to convert variables.

Tree height size spectrum.—Fig. 7a shows the robustness of the AMS3D approach to estimate the H size-abundance relationships over heterogeneous forest plots. For instance, plot A1 is characterized by the lowest number of small trees and a large number of tall trees and has been properly characterized by the AMS3D when compared with the field inventory.

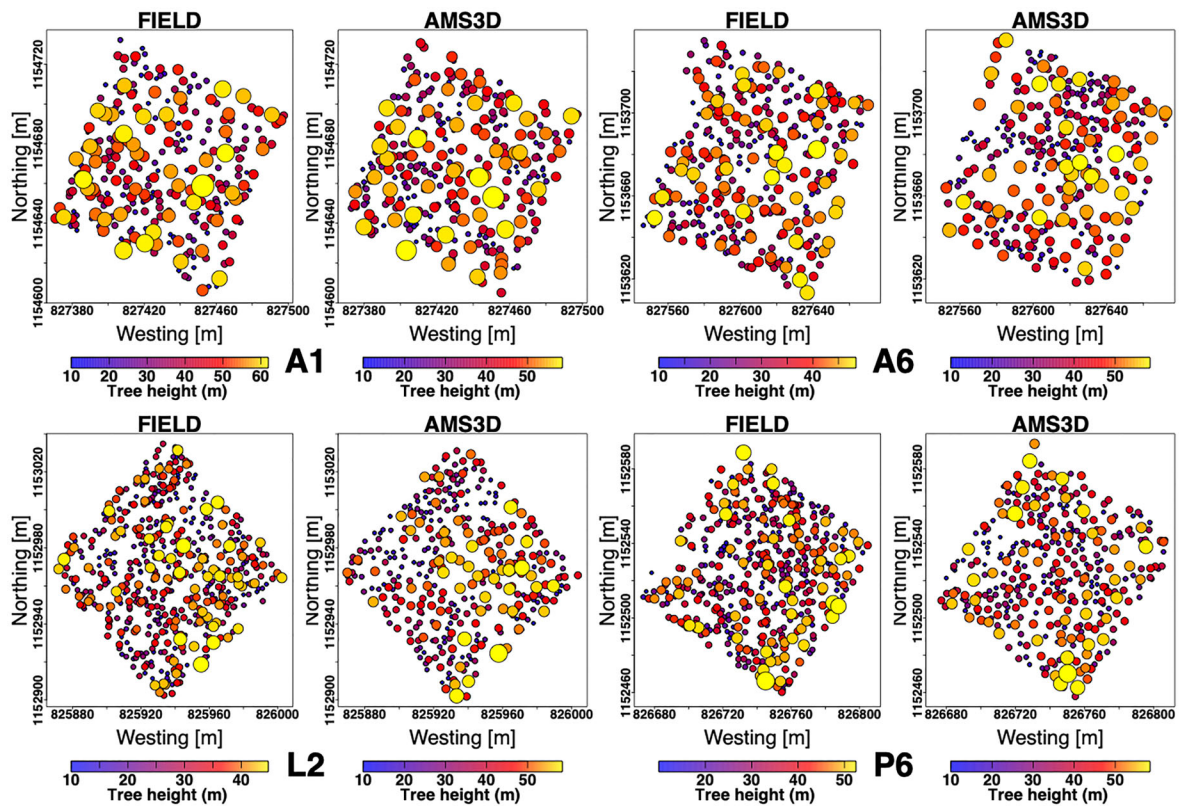


FIG. 5. Examples of tree height (H) distribution maps comparing field and AMS3D inventory. H variability is given by the color map whereas the size of the dots has been assigned to 10% of the real H value for visualization purposes. Appendix S1: Figs. S7 and S8 provide distribution maps of H and tree diameter (D) over the nine 1-ha plots.

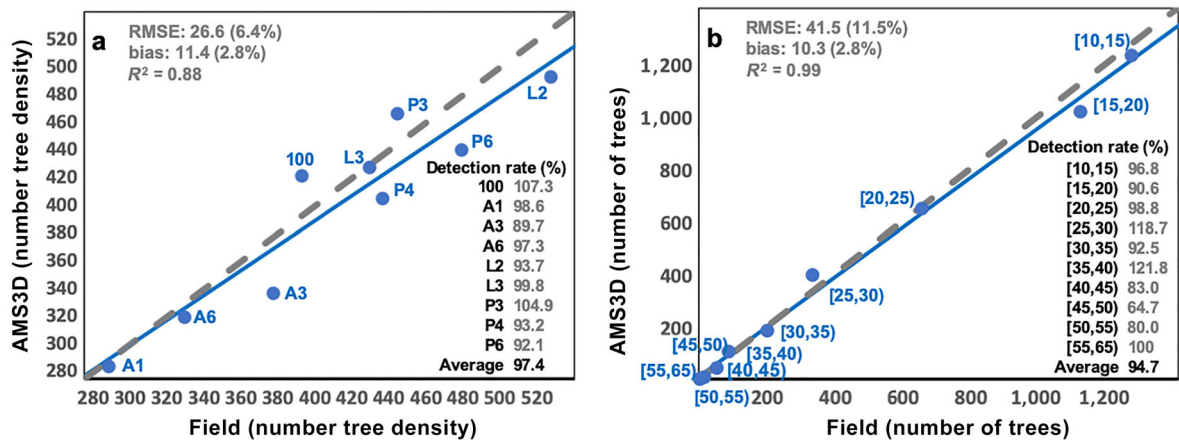


FIG. 6. Field vs. AMS3D tree density (tree height > 10 m) at the (a) plot- and (b) height-classes-level. The RMSE, bias, and the Pearson correlation coefficient of the regression model (blue line) are also shown. Negative bias means that the AMS3D overestimates the number of trees observed in the field. The tables show the detection rates (%) where values higher than 100% mean that the AMS3D overestimates the number of trees. Plot-level tree density retrievals without applying the H correction factor are shown in Appendix S1: Figs. S4 and S5.

The ASM3D was also able to capture the size spectra of plots L2 and P6 that are structurally different from A1 as they have relatively fewer tall trees and the largest number of small trees in the area. In general, field and AMS3D approaches describe similar turnover points (i.e., the height value where two given size spectra cross each other) that define the height intervals where each plot dominates in terms

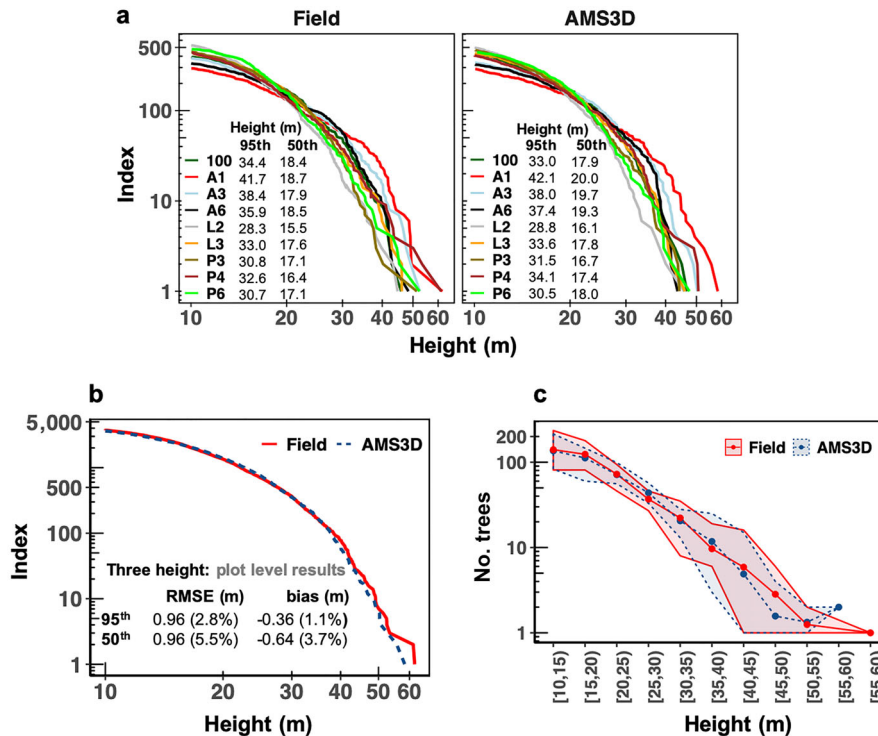


FIG. 7. Tree height (H) (a) plot-level spectra and tables with the 95th and 50th percentile of individual tree H and (b) landscape-level spectra calculated considering all the trees within the nine 1-ha plots. The statistics (RMSE and bias) in panel b are calculated from the plot-level results on the 95th and 50th percentiles shown in panel a (refer to Appendix S1: Section S7 and Fig. S9 for details). The negative bias means that the field observation underestimates the AMS3D findings. (c) The average (dots) and range (minimum and maximum shown by the shaded areas) of number of trees within the nine 1-ha plots according to size classes. Graphs in panels a and b are on a log x –log y scale, panel c is shown on a log y scale.

of number of individuals. The turnover points average $H \sim 27$ m (they range between 22 m and 30 m) that we found to be a landscape-level proxy for the height threshold that divides the lower canopy from the upper canopy (medium-spaced crowns) that contains the crowns of the trees that are driving biomass stocks in La Selva (Meyer et al. 2018).

Results from the landscape-level size spectra indicate that the AMS3D distribution is unbiased as the profiles overlap for nearly the entire size spectrum with a slight shift for trees $H > 40$ m indicating larger errors in the domain of the large trees (Fig. 7b). However, plot-level errors are not significant as the 95th percentile of individual tree H estimated from the AMS3D trees has relatively small error (RMSE = 0.96 m or 2.8%,) with no bias (-0.36 m, or 1.1%, Fig. 7b). The 50th percentile have slightly higher error and bias (RMSE = 5.5% and bias = -3.7%) suggesting that the AMS3D provides unbiased landscape-level metrics and indexes related with H (e.g., Lorey's mean height). Fig. 7c shows that the average and range of tree density strongly agrees with the field inventory for every H class of 5 m interval. The results indicate that the methodology can be used to replace large-scale ground inventory plots by providing

reliable tree size and density information from local to regional scales.

Crown area size spectrum.—The relationship between the field and AMS3D estimates on the plot-level CA spectra hold fairly strong (Fig. 8a). For instance, both approaches estimate A1 as the plot with the lowest number of trees with small crowns and the largest density of large tree crowns. Plot 100 has the largest number of small crowns and the density of large crowns is within the average for both approaches. However, CA spectra in terms of magnitude are significant (Fig. 8). Both approaches agree in estimating the plot-level CA 90th percentile (RMSE = 15% and bias = 0.8%, Fig. 8b) but they diverge for the remaining crown sizes. The landscape-level spectra shown in Fig. 8b cross each other around $CA = 90$ m² indicating that the AMS3D finds smaller crowns for the vast majority of the trees ($\sim 90\%$) and larger crowns for a small fraction ($\sim 10\%$).

Many reasons contribute for the underestimation of small crowns by the lidar approach. Understory crowns are typically underrepresented in the point cloud because a significant amount of the lidar energy is reflected by the dense upper canopy, the so-called lidar

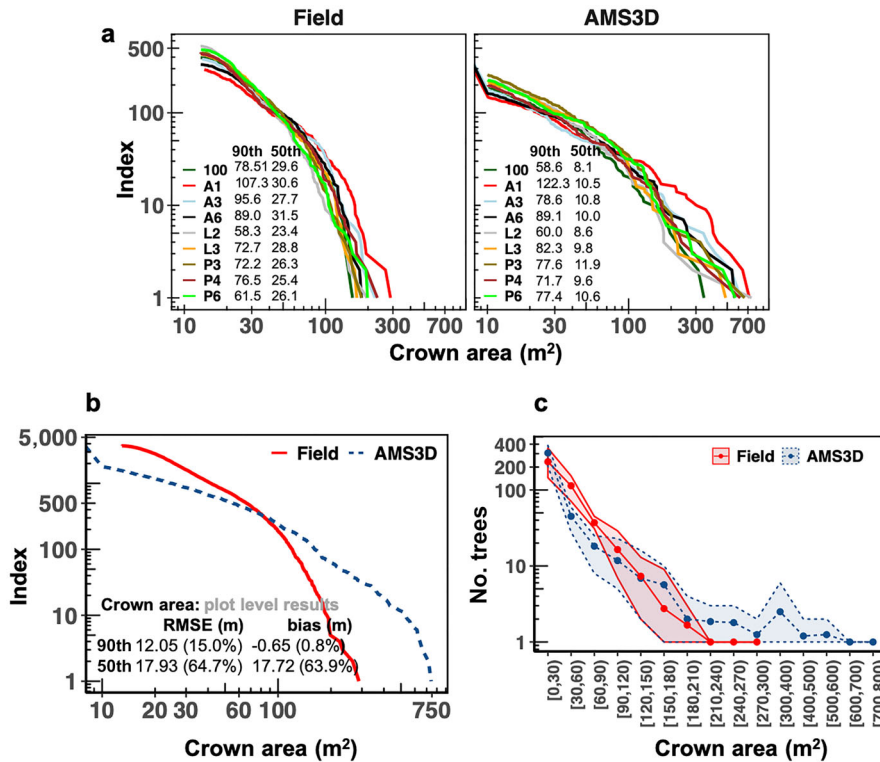


FIG. 8. Crown area (CA) (a) plot-level spectra and tables with the 90th and 50th percentile of individual trees CA and (b) landscape-level spectra calculated considering all the trees within the nine 1-ha plots. The statistics (RMSE and bias) in panel b are calculated from the plot-level results on the 95th and 50th percentiles shown in panel a (refer to Appendix S1: Section S7 and Fig. S10 for details). Negative bias means that the AMS3D findings are larger than the field inventory observations. (c) The average (dots) and range (minimum and maximum shown by the shaded areas) of number of trees within the nine 1-ha plots according to size classes. The bins have different sizes for visualization purposes. Graphs in panels a and b are on a log x -log y scale, panel c is shown on a log y scale.

occlusion effect (Korpela et al. 2012). Note that, the AMS3D accurately estimates the tree density and H of understory trees regardless of the poor representation of their crown shapes (Figs. 6 and 7). The characterization of underneath crowns might be improved by optimizing the lidar flight parameters to increase the point density in the understory layers. For instance, large scan angles increase the likelihood of the laser beams to penetrate the vegetation by traveling through vegetation gaps (Morsdorf et al. 2008, Detto et al. 2015) and decreasing the flight altitude increases the lidar power and the echo-triggering probabilities in the understory (Korpela et al. 2012). However, the magnitude of such improvements it stills unclear because most photons are reflected by the dense top canopy layer regardless of the lidar flight configuration. Alternatively, more studies have focused on integrating terrestrial and airborne laser scanning to mitigate the occlusion effect and reducing uncertainties associated with measuring CA from the field (Hancock et al. 2017, Stovall and Shugart 2018, Disney et al. 2019, Schneider et al. 2019). While encouraging, terrestrial lidar data acquisition is time- and labor-intensive, it requires ground access to the areas of

study and cannot be obtained at regional or continental studies.

Results show the opposite pattern for the larger crowns, with the AMS3D finding much larger CA compared with the field technique. Both approaches use a two-step procedure to estimate CA. The field technique collects crown size estimates for a subsampling of the trees ($n = 285$, Fig. 9a) in order to establish allometric models that enable the estimation of CA for all the trees within the study area ($n = 3723$, Fig. 9c). The lidar method extracts trees from a canopy height model ($n = 791$, Fig. 9b) to establish its own allometric model (Fig. 2) that is then used to calibrate the AMS3D algorithm that computes three-dimensional clusters used to estimate the CA for each individual tree crown ($n = 3620$, Fig. 9d). The field and lidar crown size sampling find similar H -CA relationships in terms of shape but with differences in magnitude (Fig. 9a, b). The field observations on CA are bounded by 300 m^2 whereas they can exceed 400 m^2 for the AMS3D. Larger differences are visible when the estimates are scaled-up to the landscape level (Fig. 9c, d). While the field-based results are bounded by the ground observations (i.e.,

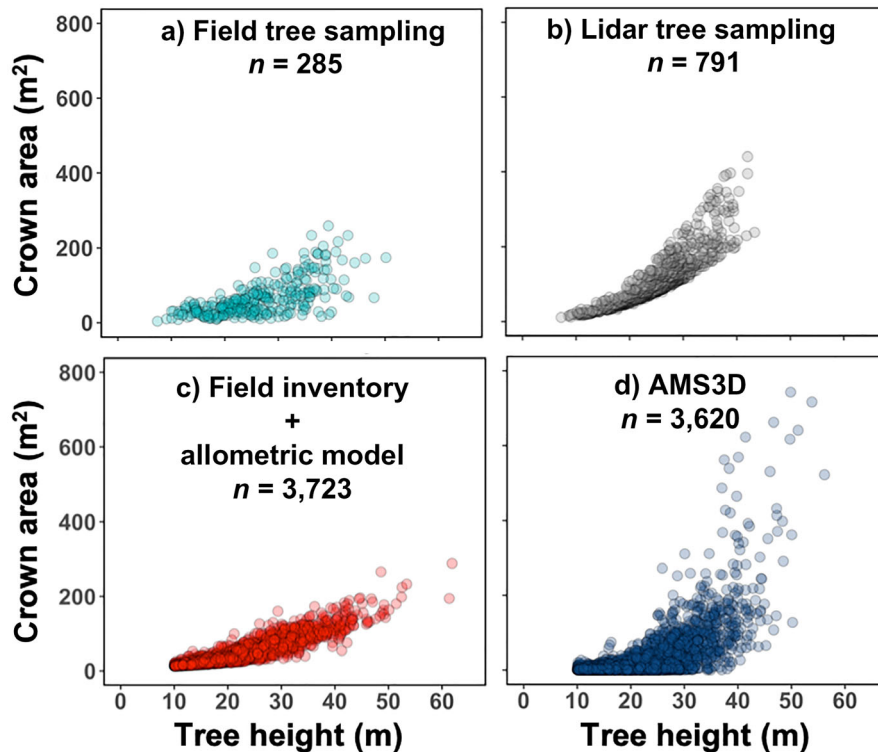


FIG. 9. Crown area (CA) plotted against tree height (H) using samples from (a) the field technique for 285 individuals and (b) the lidar-based method for 791 individuals (Fig. 2, see *Airborne lidar observation and tree crown extraction*). Estimates for all the trees within the study area (c) from ground observations together with field allometry and (d) from the AMS3D are also shown.

$0 < CA < 300 \text{ m}^2$), the AMS3D expands significantly the variability of CA ($0 < CA < 800 \text{ m}^2$, Fig. 9d) compared to the tree sampling (Fig. 9b) showing that the lidar approach is driven by forest structure characteristics rather than by the allometry used to calibrate the AMS3D.

We compare our findings with field measurements acquired over different tropical forests to investigate the similarities and discrepancies with CA distributions calculated by the field and AMS3D approaches over our study site. Blanchard et al. (2016) reports field-based CA on 4,148 individuals (located over rain forests of French Guiana, Cameroon, Gabon, and Indonesia) that can reach up to 800 m^2 . Field inventories in Barro Colorado Island (BCI), Panama (Bohman and O'Brien 2006), Brazilian Amazon (Longo et al. 2016), and Peru (Goodman et al. 2014) measured 1,594, 17,072, and 51 specimens and report CA ranging from 1 to $1,090 \text{ m}^2$, 0.03 to 1100 m^2 , and 17 to 996 m^2 , respectively. Therefore, these results agree rather with the findings of the AMS3D approach as large crowns are a common characteristic of emergent and dominant trees in old-growth forest. As with the AMS3D approach, results in BCI and Peru estimate a relationship in which CA saturates with increasing H , whereas our field estimates are in accordance with Brazilian Amazon sampling that found a linear allometric equation with no saturation (see

Appendix S1: Fig. S13). In Aubry-Kientz et al. (2019), our approach is compared to five methods that delineate crowns for the topmost trees visible in a canopy height model (CHM) over French Guiana. The AMS3D found consistent results in terms of CA and tree density outperforming the remaining methods. The reference crowns, delineated visually using a CHM and optical imagery, can reach more than 800 m^2 .

Tree diameter size-frequency, basal area, and biomass.—The tree D size-abundance profiles calculated using the AMS3D approach strongly agree with the field observations across different forest structures (Fig. 10a). Plots dominated by large D trees and the lowest number of small D stems were consistently represented by the AMS3D approach (e.g., plot A1 and A3). Plots L2 and P6 show the opposite pattern with the largest number of small D trees while their size spectra profiles decrease faster than the remaining plots with increasing D . The turnover points (the D size where two size spectra cross each other) is within 30 cm and 60 cm and in good agreement for both techniques.

At the landscape level, the shape of the AMS3D size spectrum strongly follows the field inventory observations with differences in the tails of the size-abundance relationship ($D < 22.5 \text{ cm}$ and $D > 90 \text{ cm}$, Fig. 10b). This small discrepancy is also visible in

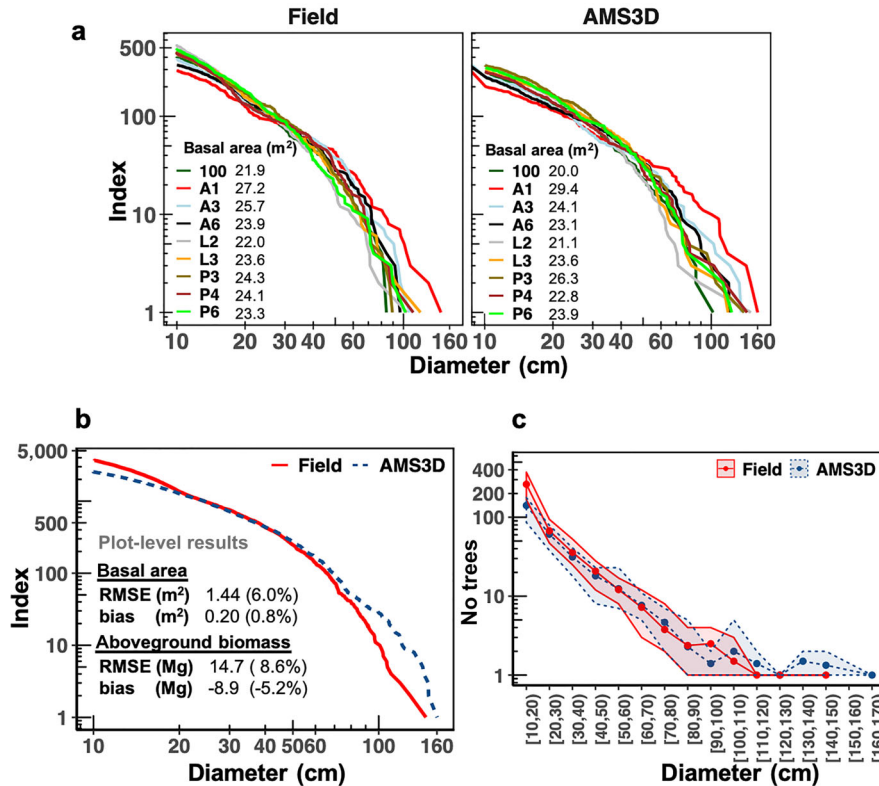


FIG. 10. Tree diameter (D) (a) plot-level spectra and tables with the plot-level basal area estimates. (b) Landscape-level spectra calculated considering all the trees within the nine 1-ha plots and statistics (RMSE and bias) for the plot-level estimates of basal area (Appendix S1: Fig. S11a) and aboveground biomass (Appendix S1: Fig. S12). Negative values mean that the AMS3D-based approach overestimated the field observations. (c) The average (dots) and range (minimum and maximum shown by the shaded areas) of number of trees within the nine 1-ha plots according to D classes. Graphs in panels a and b are on a log x -log y scale; panel c is shown on a log y scale.

Fig. 10c, which shows the average and range of number of trees within the nine 1-ha plots according to D classes. While the field approach allocates a larger number of trees to the small size domain compared with the AMS3D, the latter finds a higher density of very large size individuals ($D > 90$ cm). The differences for the very large trees are mainly related with the limitation of allometric models to explain how the D varies with remaining tree traits (H and CA) as large trees do not follow any model (Putz et al. 1983, Muller-Landau et al. 2006b, Goodman et al. 2014, see *Tree size allometry*) and, to the large uncertainties associated with measuring D above the buttress in the field (Chave et al. 2005). We expect significantly lower uncertainties associated with estimating H and CA from the AMS3D approach because most of the dominant and emergent crowns growth in isolation and are well represented in the lidar point cloud. Conversely, the discrepancy observed for small D trees is mainly related with the lidar inability to provide accurate CA estimates of small understory tree crowns. The uncertainty associated with estimating CA for small crowns using allometric models is less significant

because the CA - D variability is significantly lower compared with large crowns (Fig. 3b).

We compare the AMS3D results to the field inventory in terms of plot-level basal area (Fig. 10a, b) and aboveground biomass (Fig. 10b and Appendix S1: Section S12). We found the mismatch at the tails of the D size spectra does not impact significantly the AMS3D basal area estimates that remain unbiased ($-0.2 m^2$ or 0.8%) and with a small error (RMSE = $1.44 m^2$ or 6%). The plot-level aboveground biomass has similar uncertainty (8.6%) but a larger bias (-5.2%) that is not significant for landscape-scale estimates (refer to Appendix S1: Section S7). The bias discrepancy between basal area and biomass estimates is related to the quadratic function used to convert D into biomass that exacerbates less significant divergences on the basal area retrievals (Appendix S1: Section S7). As for the height classes results, the AMS3D findings are also strongly correlated with the field measurements (Fig. 11). The errors in estimating basal area and biomass are similar (RMSE of $\sim 22\%$) and the bias is slightly larger for biomass compared to basal area (-2.1% vs. 1.3%).

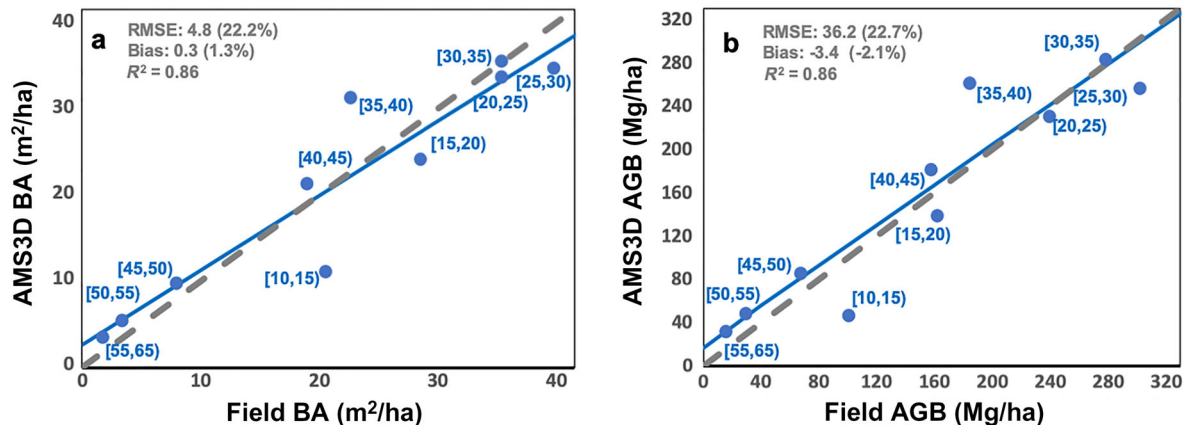


FIG. 11. Field vs. AMS3D (a) basal area (BA) and (b) aboveground biomass (AGB) for tree height classes. The RMSE, bias and the Pearson correlation coefficient of the regression model (blue lines) are also shown. Negative bias means that the AMS3D overestimates the number of trees observed in the field.

We find that AMS3D has the potential to provide unbiased basal area and biomass estimates at the plot and size level over large areas that is critically needed for many landscape-scale ecological studies such as quantifying forest successional trajectory, productivity, tree mortality, or different structural traits across edaphic and climate gradients (Brown et al. 1989, Clark and Clark 2000, Souza et al. 2019). The AMS3D is the first tool to provide direct retrieval of plot-level basal area and aboveground biomass using an approach conceptually similar to field inventory measurements and estimates. We expect by further examination of the tool in different forest types and evaluation of its performance across biomass ranges, it can be used operationally to overcome the difficulty and limitations of using field forest inventory samples across large extent of intact tropical forests for either direct estimation of biomass or for area-based calibration of lidar data (Jucker et al. 2017).

Impact of allometric equations on tree diameter and basal area estimates.—Airborne remote sensing techniques rely on allometric models to estimate D as tree stems are not visible from nearly nadir looking platforms. We show that the selection of the allometry is critical to derive D size distributions by comparing three local models to a pantropical allometric equation (Fig. 12). The first model that estimates D from both H and CA (refer to *Tree diameter size–frequency, basal area, and biomass*, Fig. 10b, c) is compared to two additional local allometric models that estimate D from H and CA separately (Fig. 12a, b and; Fig. 12c, d, respectively). The pantropical method has been derived by Jucker et al. (2017) using field inventories across the Neotropical geographical region (Fig. 12e, f).

The D spectra calculated from the models defined as a function of $H \times CA$ and CA alone agree for the mid-size trees ($22.5 < D < 90$ cm), whereas estimates using the $D-H$ allometry has better results for the tails of the

spectra. The model used for Neotropical trees provides reasonable estimates for a small interval within the mid-range size trees ($22.5 \text{ cm} < D < 35 \text{ cm}$) but it fails for the remaining spectra. Our results agree with the literature that emphasizes the importance of using local allometry as opposed to pantropical equations in the framework of many applications (e.g., basal area, biomass, and carbon stocks; Feldpausch et al. 2011, Malhi et al. 2006, Paoli et al. 2008, Saatchi et al. 2015). The lidar ITC approach can play a major role in developing local allometry (e.g., $D-H$ and $D-CA$) across forest types. Our results also suggest that using multiple allometry models for different diameter range may prove to be more reliable to predict the entire diameter spectra accurately. By comparing Figs. 10b and 12a, we conclude that the $H-D$ allometry better explains the size of small and very large trees, whereas the models based on both H and CA are better suited to predict the D of mid-size trees.

The basal area estimates support these conclusions as the neotropical model has the highest bias ($\sim 16\%$) and largest error (RMSE = 20.3%, Fig. 12e). The local models that depend on two tree traits prevail over the allometry defined as a function of a single trait. The models calculated from the $H-D$ allometry have a high predictive power (Appendix S1: Fig. S12d) but results are biased with a significant error (RMSE = 15% and bias 14%, Fig. 12a), whereas the estimates based on the $CA-D$ allometry are nearly unbiased, they have a smaller error (RMSE = 10% and bias = 3%, Fig. 12b) but the basal area variability is poorly explained (Appendix S1: Fig. S12c). The best model is defined as a function of two structural variables (i.e., $H \times CA$, RMSE = 6%, bias = 0.8%, Fig. 10b). These results highlight the need for allometric equations calibrated from more than a single tree trait and the relevance of observations on CA that are usually not measured in the field inventories.

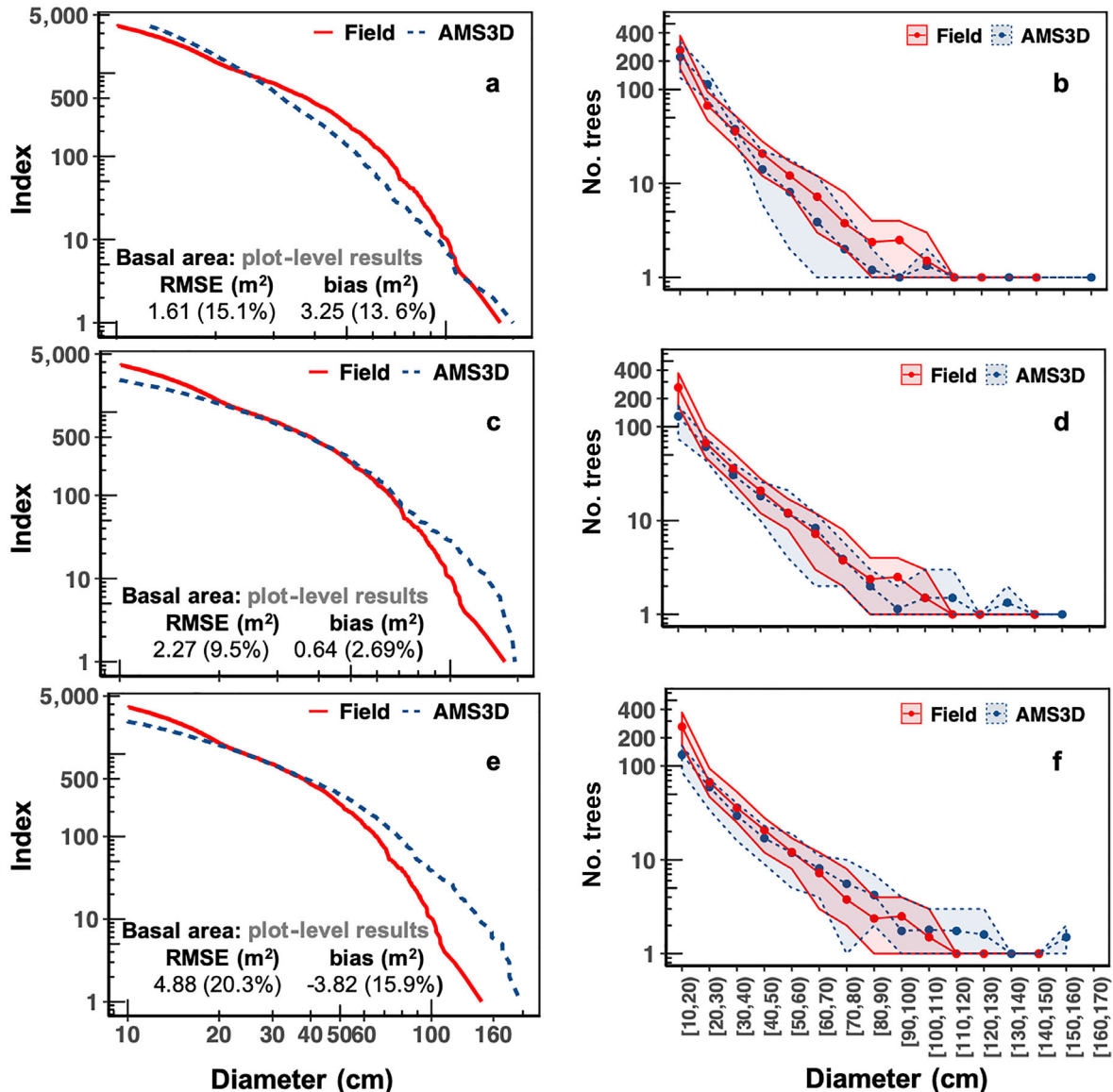


FIG. 12. Tree diameter (D) results regarding (a, c, e) size spectra and (b, d, f) averaged (dots) and range (minimum and maximum represented by the shaded areas) of number of trees within the 1-ha plots. D has been converted from AMS3D-derived traits using (a, b) $D = 7.42 \times \exp(0.05 \times H)$ (Appendix S1: Eq. S7), (c, d) $D = 4.03 \times CA^{0.55}$ (Appendix S1: Eq. S4), and (e, f) a neotropical allometric equation Appendix S1: (Eq. S16; Jucker et al. 2017). The development of the local allometry used in panels a–d is explained in Appendix S1: Section S6. The statistics (RMSE and bias) of the basal area estimates are also provided (refer to Appendix S1: Fig. S11 for details). Graphs in the left and right column are on a log x –log y and log y scale, respectively.

Variation of tree size–frequency distributions across forest types

Fig. 13a shows probability density functions of tree density calculated by the AMS3D over 1-ha plots that have been systematically sampled over a variety of forest types (Fig. 1). We calculated the average number of trees according to forest types and size classes of H and crown radius (CR, Fig. 13b, c, CR has been preferred to CA for visualization purposes). Forested swamps have the

lowest tree density because of tall trees predominance with relatively few individuals in the understory. Selectively logged forests have a higher tree density compared with old-growth forest due to the large number of individuals involved in the forest succession that occurs in the gaps created by tree removal activities (Brokaw 1985). The old-growth forest distribution is bimodal centered on ~ 300 trees/ha and ~ 400 trees/ha. According to the field inventory, the tree density distribution is centered on 400 trees/a (average = 413, minimum = 293,

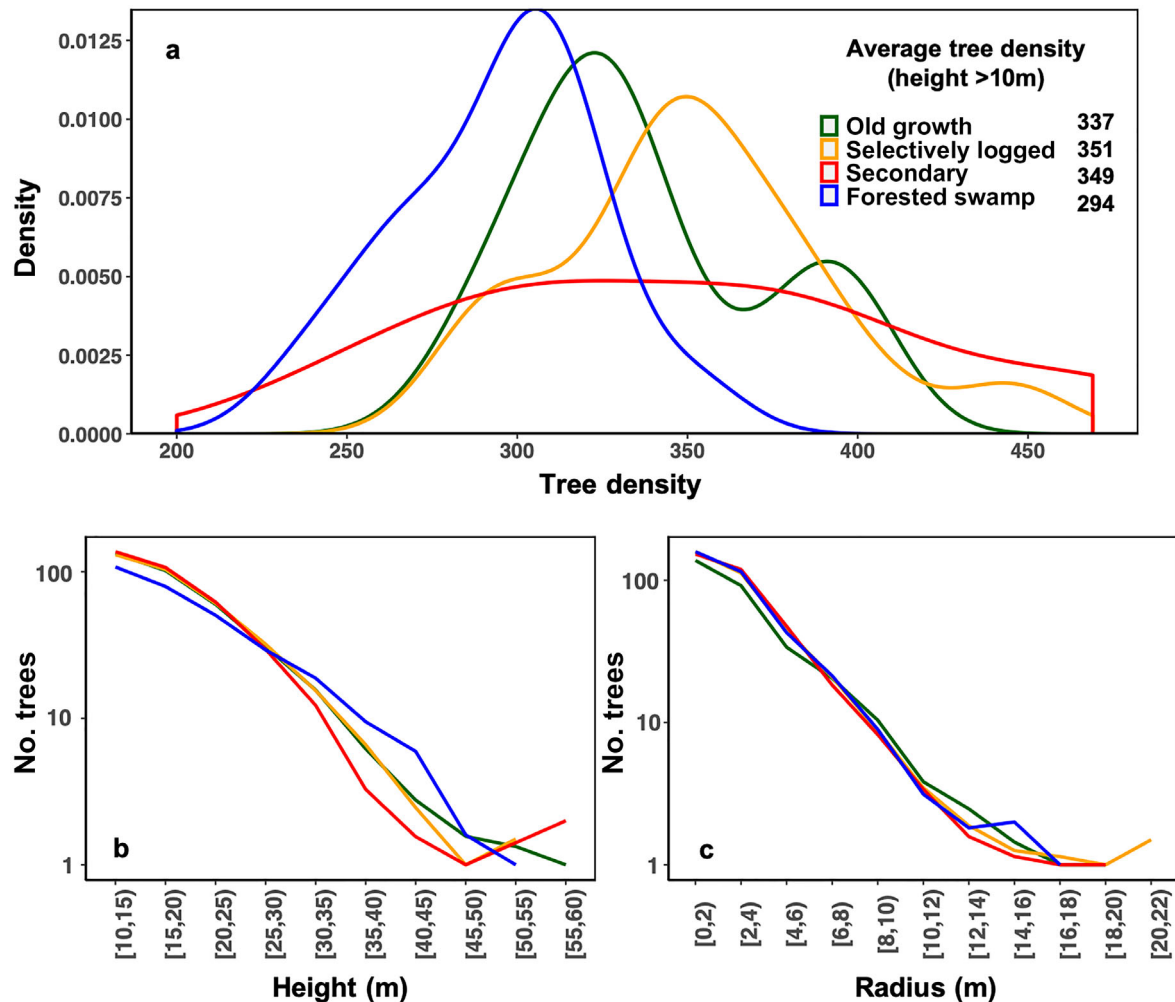


FIG. 13. AMS3D results over 1-ha plots defined using a systematic sampling over different forest types (Fig. 1). (a) Probability density function (PDF) and average tree density by forest type. The graph in panel a is limited to range between 200 and 500 trees/ha for visualization purposes. Average number of trees by forest type and according to size classes of (b) tree height and (c) crown radius. Crown radius has been preferred to crown area for visualization purposes. Panels b and c are shown on a log y scale.

maximum = 527 trees/ha) with no local mode on 300 trees/ha. Field plots are located over areas with favorable conditions compared with the lidar measurements that span over large variability of edaphic and topographic conditions across La Selva. The lidar covers areas located in higher altitudes and many forest patches are located close to the edges with different forest types (e.g., secondary forest) that might impact the structure of the forest (Fig. 1 and Appendix S1: Fig. S1). Secondary forests do not have a dominant tree density suggesting the existence of a large variety of successional stages.

The average number of trees by H class in selectively logged forests closely follows the old-growth profile except for trees with $H > 40$ m that might be explained by the fact that logging activities target large trees (Fig. 13b). The tree density profile of the secondary forest matches the old-growth and selectively logged

profiles up to 25 m in H but it drops significantly for taller trees. However, secondary forests dominate in number of trees taller than 45 m due to remnant trees left after clearing that have grown with no competition for resources. Swamp forests have the lowest number of short trees, have no trees among the tallest trees in the region but dominate in number of trees in the range of $35 \text{ m} < H < 45 \text{ m}$.

The variability in the average number of trees by CR class is significantly lower compared to the H classes (Fig. 13c). As expected, old-growth forests have a lower average number of small trees compared with the remaining forest types. It suggests that the AMS3D successfully characterizes shade-tolerant understory species that invest in expanding the crowns rather than in H . The largest crowns are located in selectively logged and secondary forests that might correspond to crowns next

to forest gaps created by the tree removal and remnant trees that could invest in crown expanding at low cost due to lack of competition.

CONCLUSION

The adaptive mean shift (AMS3D) lidar individual tree crown (ITC) mapping explained 88% of plot-level (1 ha) tree density variability (tree height > 10 m) with nearly no bias (2.8%). The tree detection rate was of $97.4\% \pm 5.6\%$ with plot-level errors bounded by 10%, making it a remarkable approach for mapping tree density over complex ecosystems. Average tree detection rates for height classes of 5-m intervals were also highly satisfactory ($94.7\% \pm 17.2\%$) but class-level errors are larger compared with the plot-level findings.

The plot-level size spectra of tree height and tree diameter closely follow the field measurements and when aggregating the ITC results to the landscape scale, the size spectra remained unbiased. Results on crown area spectra were less impressive. We found that airborne lidar systems are more suitable to measure canopy crowns than field techniques, with the caveat of underestimating the understory crowns, where ground measurements may be more accurate. The performance of the airborne lidar technology over understory trees may improve significantly with higher lidar point densities acquired from manned or unmanned aircrafts or the measurements are combined with terrestrial lidar measurements.

We found unbiased and low error plot-level basal area (RMSE = 6%, bias = 0.8%) and aboveground biomass (RMSE = 9%, bias = -5.2%) estimates by converting the lidar ITC metrics (tree height and crown area) into tree diameter and biomass using field allometric models. Results for tree height classes (5-m intervals) have higher errors (RMSE of 22% and 23%) but remain unbiased (1.3% and -2.1%) for basal area and biomass, respectively. These results are extremely encouraging as it enables the estimation of basal area and carbon stocks at scale covering large areas with diverse topographic, edaphic, climate and forest disturbance gradients that are critically needed to address regional and global ecological applications. The AMS3D overcomes the limitations of area-based approaches that require extensive field sampling to calibrate for the regional variability between lidar metrics (e.g., top of the canopy height) and biophysical metrics (e.g., basal area, carbon stocks) with larger deviations verified over highly dense tropical forests.

We would like to emphasize that the evaluation of lidar AMS3D performance was only achievable because of the availability of a very detailed and comprehensive field inventory data at the La Selva Biological Station. On the one hand, the ground measurements on height for every specimen were crucial to validate our results in terms of number of trees by plot and size class. We identified a bias between field and lidar tree height estimates

that was corrected using a new approach based on ranked Q-Q plots. On the other hand, the field inventory provided a large sampling of crown size that was used to develop new local allometric models to estimate tree diameter from lidar-derived tree traits (height and crown area). We concluded that the local allometry was determinant to compare field and lidar size distributions (e.g., tree diameter, basal area, and biomass) as opposed to general allometric models that have larger uncertainties locally.

ACKNOWLEDGMENTS

The research was supported by the National Aeronautics and Space Administration (NASA) Terrestrial Ecology grant (WBS: 596741.02.01.01.67) at the Jet Propulsion Laboratory, California Institute of Technology under a contract with the NASA and partial funding to the UCLA Institute of Environment and Sustainability from previous NASA and National Science Foundation (NSF) grants. Marcos Longo was supported by the NASA Postdoctoral Program, administered by Universities Space Research Association under contract with NASA. We thank the staff of La Selva Biological Station and the Organization of Tropical Studies (OTS) for their field support.

LITERATURE CITED

- Aubry-Kientz, M., R. Dutrieux, A. Ferraz, S. Saatchi, H. Hamraz, J. Williams, D. Coomes, A. Piboule, and G. Vincent. 2019. Individual tree crowns delineation algorithms from ALS data in tropical forests. *Remote Sensing* 11:1–21.
- Banin, L., T. R. Feldpausch, O. L. Phillips, T. R. Baker, J. Lloyd, E. J. M. M. Arets, N. J. Berry, and M. Bradford. 2012. What controls tropical forest architecture? Testing environmental, structural and floristic drivers. *Global Ecology and Biogeography* 21:1179–1190.
- Baskerville, G. L. 1972. Use of logarithmic regression in the estimation of plant biomass. *Canadian Journal of Forest Research* 2:49–53.
- Bawa, K., L. McDade, and H. Hespenheide 1994. Introduction: Ecology and natural history of a neotropical rainforest. Pages 3–6 in *A. McDade, K. Bawa, H. Hespenheide, and S. Gary, editors. La Selva, ecology and natural history of a neotropical rain forest. University of Chicago Press, Chicago, Illinois, USA.*
- Blanchard, E., et al. 2016. Contrasted allometries between stem diameter, crown area, and tree height in five tropical biogeographic areas. *Trees—Structure and Function* 30:1953–1968.
- Bohlman, S., and S. O'Brien. 2006. Allometry, adult stature and regeneration requirement of 65 tree species on Barro Colorado Island, Panama. *Journal of Tropical Ecology* 22:123–136.
- Brokaw, N. V. L. 1985. Gap-phase regeneration in a tropical forest. *Ecology* 66:682–687.
- Brown, S. 1997. Estimating biomass and biomass change of tropical forests: a primer. In *For the food and agriculture organization of the united nations. Rome: FAO Forestry Paper* – 134.
- Brown, S., A. Gillespie, and A. Lugo. 1989. Biomass estimation methods for tropical forests with applications to forest inventory data. *Forest Science* 35:881–902.
- Bustamante, M. M., et al. 2016. Toward an integrated monitoring framework to assess the effects of tropical forest degradation and recovery on carbon stocks and biodiversity. *Global Change Biology* 22:92–109.
- Cano, I. M., H. C. Muller-landau, S. J. Wright, S. A. Bohlman, and S. W. Pacala. 2019. Tropical tree height and crown allometries for the Barro Colorado Nature Monument, Panama: a comparison of alternative hierarchical models

- incorporating interspecific variation in relation to life history traits. *Biogeosciences* 16:847–862.
- Chave, J., et al. 2005. Tree allometry and improved estimation of carbon stocks and balance in tropical forests. *Oecologia* 145:87–99.
- Chave, J., et al. 2014. Improved allometric models to estimate the aboveground biomass of tropical trees. *Global Change Biology* 20:3177–3190.
- Clark, D. B., D. A. Clark, S. F. Oberbauer, and J. R. Kellner. 2017. Multidecadal stability in tropical rain forest structure and dynamics across an old-growth landscape. *PLoS ONE* 12:1–20.
- Clark, D. B., D. A. Clark, and J. M. Read. 2010. Edaphic variation and the mesoscale distribution of tree species in a neotropical rain forest. *Journal of Ecology* 86: 101–112.
- Clark, D. B., and D. A. Clark. 2000. Landscape-scale variation in forest structure and biomass in a tropical rain forest. *Forest Ecology and Management* 137:185–198.
- Coomes, D., R. Duncan, R. Allen, and J. Truscott. 2003. Disturbances prevent stem size-density distributions in natural forests from following scaling relationships. *Ecology Letters* 6:980–989.
- Crowther, T. W., et al. 2015. Mapping tree density at a global scale. *Nature* 525:201–205.
- De Souza, F. C., et al. 2019. Evolutionary diversity is associated with wood productivity in Amazonian forests. *Nature Ecology and Evolution* 3:1754–1761.
- Detto, M., G. Asner, H. Muller-landau, and O. Sonnentag. 2015. Spatial variability in tropical forest leaf area density from multireturn lidar and modeling. *Journal of Geophysical Research* 120:294–309.
- Disney, M., A. Burt, K. Calders, C. Schaaf, and A. Stovall. 2019. Innovations in ground and airborne technologies as reference and for training and validation: Terrestrial Laser Scanning (TLS). *Surveys in Geophysics* 40:937–958.
- Drake, J. B., R. O. Dubayah, D. B. Clark, R. G. Knox, J. B. Blair, M. A. Hofton, R. L. Chazdon, J. F. Weishampel, and S. Prince. 2002. Estimation of tropical forest structural characteristics, using large-footprint lidar. *Remote Sensing of Environment* 79:305–319.
- Enquist, B. J., and K. J. Niklas. 2001. Invariant scaling relations across tree-dominated communities. *Nature* 410:655–660.
- Enquist, B. J., G. B. West, and J. H. Brown. 2009. Extensions and evaluations of a general quantitative theory of forest structure and dynamics. *Proceedings of the National Academy of Sciences USA* 106:7046–7051.
- Farrior, C. E., S. A. Bohlman, S. Hubbell, and S. W. Pacala. 2016. Dominance of the suppressed: Power-law size structure in tropical forests. *Science* 351:155–157.
- Feldpausch, T. R., et al. 2011. Height-diameter allometry of tropical forest trees. *Biogeosciences* 8:1081–1106.
- Ferraz, A., S. Saatchi, C. Mallet, and V. Meyer. 2016. Lidar detection of individual tree size in tropical forests. *Remote Sensing of Environment* 183:318–333.
- Fisher, R. A., et al. 2018. Vegetation demographics in Earth System Models: A review of progress and priorities. *Global Change Biology* 24:35–54.
- Goodman, R., O. Phillips, and T. Baker. 2014. The importance of crown dimensions to improve tropical tree biomass estimates. *Ecological Applications* 24:680–698.
- Hancock, S., K. Anderson, M. Disney, and K. J. Gaston. 2017. Measurement of fine-spatial-resolution 3D vegetation structure with airborne waveform lidar: Calibration and validation with voxelised terrestrial lidar. *Remote Sensing of Environment* 188:37–50.
- Hunter, M. O., M. Keller, D. Victoria, and D. C. Morton. 2013. Tree height and tropical forest biomass estimation. *Biogeosciences* 10:8385–8399.
- Iwasa, Y., D. Cohen, and J. A. Leon. 1985. Tree height and crown shape, as results of competitive games. *Journal of Theoretical Biology* 112:279–297.
- Jucker, T., et al. 2017. Allometric equations for integrating remote sensing imagery into forest monitoring programmes. *Global Change Biology* 23:177–190.
- Kitajima, K., S. S. Mulkey, and S. J. Wright. 2005. Variation in crown light utilization characteristics among tropical canopy trees. *Annals of Botany* 95:535–547.
- Korpela, I., A. Hovi, and F. Morsdorf. 2012. Understory trees in airborne LiDAR data—Selective mapping due to transmission losses and echo-triggering mechanisms. *Remote Sensing of Environment* 119:92–104.
- Larjavaara, M., and H. C. Muller-Landau. 2013. Measuring tree height: a quantitative comparison of two common field methods in a moist tropical forest. *Methods in Ecology and Evolution* 4:793–801.
- Lau, A., C. Martius, H. Bartholomeus, A. Shenkin, T. Jackson, Y. Malhi, M. Herold, and L. Patrick. 2019. Estimating architecture-based metabolic scaling exponents of tropical trees using terrestrial LiDAR and 3D modelling. *Forest Ecology and Management* 439:132–145.
- Levine, N. M., et al. 2016. Ecosystem heterogeneity determines the ecological resilience of the Amazon to climate change. *Proceedings of the National Academy of Sciences USA* 113:793–797.
- Longo, M., M. Keller, M. N. Dos-Santos, V. Leitold, E. R. Pinagé, A. Baccini, S. Saatchi, E. M. Nogueira, M. Batistella, and D. C. Morton. 2016. Aboveground biomass variability across intact and degraded forests in the Brazilian Amazon. *Global Biogeochemical Cycles* 30:1639–1660.
- Longo, M., et al. 2018. Ecosystem heterogeneity and diversity mitigate Amazon forest resilience to frequent extreme droughts. *New Phytologist* 219:914–931.
- Malhi, Y., et al. 2006. The regional variation of aboveground live biomass in old-growth Amazonian forests. *Global Change Biology* 12:1107–1138.
- McDowell, N., et al. 2018. Drivers and mechanisms of tree mortality in moist tropical forests. *New Phytologist* 219:851–869.
- Meyer, V., S. Saatchi, D. B. Clark, M. Keller, G. Vincent, A. Ferraz, F. Espírito-Santo, M. V. N. D'Oliveira, D. Kaki, and J. Chave. 2018. Canopy area of large trees explains above-ground biomass variations across neotropical forest landscapes. *Biogeosciences* 15:3377–3390.
- Molto, Q., M. Daullet, A. Rousteau, and V. Rossi. 2014. Predicting tree heights for biomass estimates in tropical forests – a test from French Guiana 11:3121–3130.
- Morsdorf, F., O. Frey, E. Meier, K. I. Itten, and B. Allgöwer. 2008. Assessment of the influence of flying altitude and scan angle on biophysical vegetation products derived from airborne laser scanning. *International Journal of Remote Sensing* 29:1387–1406.
- Muller-Landau, H., et al. 2006a. Testing metabolic ecology theory for allometric scaling of tree size, growth and mortality in tropical forests. *Ecology Letters* 9:575–588.
- Muller-Landau, H., et al. 2006b. Comparing tropical forest tree size distributions with the predictions of metabolic ecology and equilibrium models. *Ecology Letters* 9:589–602.
- Negrón-Juárez, R. I., et al. 2018. Vulnerability of Amazon forests to storm-driven tree mortality. *Environmental Research Letters* 13. <https://iopscience.iop.org/article/10.1088/1748-9326/aabe9f>
- Nobre, C. A., G. Sampaio, L. S. Borma, J. C. Castilla-rubio, J. S. Silva, and M. Cardoso. 2016. Land-use and climate change

- risks in the Amazon and the need of a novel sustainable development paradigm. *Proceedings of the National Academy of Sciences USA* 113:10759–10768.
- Nogueira, E., B. Walker, and P. Fearnside. 2006. Volume and biomass of trees in central Amazonia: influence of irregularly shaped and hollow trunks. *Forest Ecology and Management* 227:14–21.
- Paoli, G. D., L. M. Curran, and F. J. Slik. 2008. Soil nutrients affect spatial patterns of aboveground biomass and emergent tree density in southwestern Borneo. *Oecologia* 155: 287–299.
- Poorter, L., F. Bongers, F. Sterck, and H. Wöll. 2003. Architecture of 53 rain forest tree species differing in adult stature and shade tolerance. *Ecology* 84:602–608.
- Putz, F. E., P. D. Coley, K. Lu, A. Montalvo, and A. Aiello. 1983. Uprooting and snapping of trees: structural determinants and ecological consequences. *Canadian Journal of Forest Research* 13:1011–1020.
- Saatchi, S., J. Mascaro, L. Xu, M. Keller, Y. Yang, P. Duffy, F. Espírito-Santo, A. Baccini, J. Chambers, and D. Schimel. 2015. Seeing the forest beyond the trees. *Global Ecology and Biogeography* 24:606–610.
- Schimel, D., F. D. Schneider, and JPL Carbon and Ecosystem Participants. 2019. Flux towers in the sky: global ecology from space. *New Phytol.* 224:570–584. <https://doi.org/10.1111/nph.15934>.
- Schneider, F. D., D. Kükenbrink, M. E. Schaepman, D. S. Schimel, and F. Morsdorf. 2019. Quantifying 3D structure and occlusion in dense tropical and temperate forests using close-range LiDAR. *Agricultural and Forest Meteorology* 268:249–257.
- Soininen, A. 2011. TerraScan User's guide. <http://www.terrasolid.com/guides/tscan/index.html>
- Stovall, A. E. L., and H. H. Shugart. 2018. Improved biomass calibration and validation with terrestrial lidar: Implications for future LiDAR and SAR missions. *IEEE Journal of Selected Topics in Applied Earth Observations and Remote Sensing*. 11:3527–3537.
- Wang, Y., M. Lehtomäki, X. Liang, J. Pyörälä, A. Kukko, A. Jaakkola, J. Liu, Z. Feng, R. Chen, and J. Hyypä. 2019. Is field-measured tree height as reliable as believed—A comparison study of tree height estimates from field measurement, airborne laser scanning and terrestrial laser scanning in a boreal forest. *ISPRS Journal of Photogrammetry and Remote Sensing* 147:132–145.
- West, G. B., B. J. Enquist, and J. H. Brown. 2009. A general quantitative theory of forest structure and dynamics. *Proceedings of the National Academy of Sciences USA* 106:7040–7045.
- White, E. P., S. K. M. Ernest, A. J. Kerkhoff, and B. J. Enquist. 2007. Relationships between body size and abundance in ecology. *Trends in Ecology and Evolution* 22:323–330.
- Yanoviak, S. P., E. M. Gora, P. M. Bitzer, J. C. Burchfield, H. C. Muller-Landau, M. Detto, S. Paton, and S. P. Hubbell. 2019. Lightning is a major cause of large tree mortality in a lowland Neotropical forest. *New Phytologist* 225:1936–1944.

SUPPORTING INFORMATION

Additional supporting information may be found online at: <http://onlinelibrary.wiley.com/doi/10.1002/eap.2154/full>

DATA AVAILABILITY

Data are available from the Dryad Digital Repository: <https://doi.org/10.5068/D17W9M>